Supplementary Materials: In Situ Studies and Magnetic Properties of the *Cmcm* Polymorph of $LiCoPO_4$ with a Hierarchical Dumbbell-Like Morphology Synthesized by Easy Single-Step Polyol Synthesis

Carlos Alarcón-Suesca, Jennifer Ludwig, Viktor Hlukhyy, Christoph Stinner and Tom Nilges

1. Structural, Physical and Chemical Properties

1.1. Rietveld Refinement Details

The background profile, which can rather be attributed to the capillaries used than to amorphous components of the material, was fitted with a Chebyshev polynomial function with 35 coefficients. Thereafter, the lattice parameters as well as the zero-point and scale factor were refined. A pseudo-Voigt profile function with three Gaussian and one Lorentzian coefficients was used for modeling the shape of the diffraction peaks; the profile was cut outside the 8 FWHM range. Because the FWHM of the peaks exhibited a marked anisotropy, anisotropic strain broadening implemented in JANA2006 [42] was tentatively refined. No correction for preferred orientation was applied. Peak asymmetry, which was especially observed at low scattering angles, was corrected by the axial divergence model described by Finger et al. [43]. The empirical starting values of the parameters S/L and H/L were set to −0.011 and 0.06, according to the characteristics of the instrument. The refinement of the general atomic positions of Co, P, and O was performed unrestrictedly, the atomic site occupancies as well as the thermal parameters were fixed. As Li positions and thermal displacement parameters cannot be deduced by means of X-ray diffraction because of the low atomic scattering factor, they have been fixed as well. After applying an absorption correction (estimated packing fraction ~0.6) [44], the temperature factors of the Co, P and O sites were refined freely. Finally, the Berar's factor was applied to obtain more realistic standard uncertainties [45].

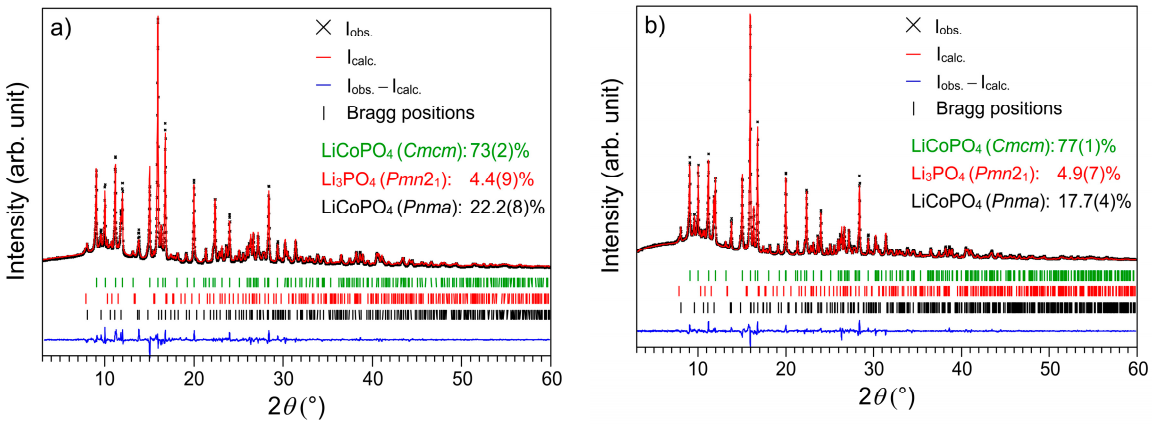

Figure S1. Rietveld fits of the X-ray powder diffraction patterns of LCP-*Cmcm* obtained from solvothermal synthesis using (**a**) TEG; and (**b**) TTEG as solvents.

Table S1. Crystallographic data, details of data collection, and structure refinement of LCP-*Cmcm* prepared by (a) solvothermal (ST) ((a) DEG, (b) TEG, and (c) TTEG solvent) and (d) polyol (PO) syntheses as refined from X-ray powder diffraction data at T = 298 K [a].

	(a) LCP (ST-DEG)	(b) LCP (ST-TEG)	(c) LCP (ST-TTEG)	(d) LCP (PO)
M_r (g·mol^{-1})		160.8		
Crystal system		orthorhombic		
Space group		*Cmcm* (no. 63)		
Z		4		
a (Å)	5.4347(4)	5.4354(5)	5.4341(4)	5.4433(3)
b (Å)	8.1638(5)	8.1680(7)	8.1676(5)	8.1694(4)
c (Å)	6.2135(4)	6.2159(5)	6.2176(4)	6.2129(3)
V (Å3)	275.68(3)	275.97(4)	275.96(3)	276.28(2)
F(000)	112	112	112	308
ρ (calcd) (g·cm^{-1})	3.8753(6)	3.8713(8)	3.8714(6)	3.8657(4)
R_p	0.032	0.041	0034	0.021
R_{wp}	0.041	0.057	047	0.027
R_{exp}	0.026	0.026	0.030	0.025
R_F	0.018	0.024	0.027	0.013
χ^2	1.57	2.16	1.57	1.08
Data/restraints/parameter	3802/0/75	3800/0/75	3800/0/75	3835/0/55
Phase composition	93(2) wt % $LiCoPO_4$ (*Cmcm*) 3.4(4) wt % $LiCoPO_4$ (*Pnma*) 4(2) wt % Li_3PO_4 ($Pmn2_1$)	73(2) wt % $LiCoPO_4$ (*Cmcm*) 22.2(8) wt % $LiCoPO_4$ (*Pnma*) 4.4(9) wt % Li_3PO_4 ($Pmn2_1$)	77(1) wt % $LiCoPO_4$ (*Cmcm*) 17.7(4) wt % $LiCoPO_4$ (*Pnma*) 4.9(7) wt % Li_3PO_4 ($Pmn2_1$)	100 wt % $LiCoPO_4$ (*Cmcm*)

[a] The estimated standard deviations (E.S.D's) were calculated by means of the Berar's procedure und are indicated in round brackets.

Table S2. Fractional atomic coordinates and isotropic thermal displacement parameters of (a) LCP-*Cmcm* (ST; from DEG), and (b) LCP-*Cmcm* (PO) as refined from X-ray powder diffraction data at T = 298 K [a].

Sample	Atom	Wyckoff Position	x/a	y/b	z/c	U_{iso} (Å^2)
LCP-*Cmcm* (ST)	Li1	4*c*	0	0.675 [b]	¼	0.019 [b]
	Co1	4*a*	0	0	0	0.0107(9)
	P1	4*c*	0	0.3527(6)	¼	0.0118(13)
	O1	8*f*	0	0.2469(6)	0.0505(11)	0.007(2)
	O2	8*g*	0.2289(9)	0.4653(8)	¼	0.006(2)
LCP-*Cmcm* (PO)	Li1	4*c*	0	0.675 [b]	¼	0.019 [2]
	Co1	4*a*	0	0	0	0.0107(5)
	P1	4*c*	0	0.3523(4)	¼	0.0064(8)
	O1	8*f*	0	0.2474(4)	0.0500(7)	0.0039(13)
	O2	8*g*	0.2255(6)	0.4653(5)	¼	0.0028(12)

[a] The estimated standard deviations (E.S.D's) were calculated by means of the Berar's procedure und are indicated in round brackets; [b] Li positions and thermal factors have been fixed as they cannot be deduced by means of X-ray diffraction due to the low atomic scattering factor.

Table S3. Selected interatomic distances in (a) LCP-*Cmcm* (ST; from DEG), and (b) LCP-*Cmcm* (PO) as refined from X-ray powder diffraction data at T = 298 K [a].

Sample	Atom Pair			d (Å)
(a) LCP-*Cmcm* (ST)	Li1	O1	×2	1.973(6)
		O2	×2	2.116(6)
	Co1	O1	×2	2.040(5)
		O2	×4	2.159(3)
	P1	O1	×2	1.511(7)
		O2	×2	1.547(6)
(b) LCP-*Cmcm* (PO)	Li1	O1	×2	1.968(4)
		O2	×2	2.107(4)
	Co1	O1	×2	2.045(3)
		O2	×4	2.174(2)
	P1	O1	×2	1.510(4)
		O2	×2	1.536(4)

[a] The estimated standard deviations (E.S.D's) were calculated by means of the Berar's procedure und are indicated in round brackets.

1.2. Infrared Spectroscopy

Attenuated total reflectance (ATR)-Fourier transform infrared spectroscopy (FTIR) data were collected on a Varian 670 IR FTIR spectrometer equipped with a PIKE GladiATR ATR stage (400–4000 cm^{-1}, 132 scans). The Agilent Resolution Pro software was used for data handling. Figure S2 shows the FT-IR spectrum of *Cmcm*-$LiCoPO_4$. Generally, the spectra of $LiCoPO_4$ polymorphs are dominated by the fundamental vibrations of the $[PO_4]^{3-}$ groups, which involve the displacement of oxygen atoms of the tetrahedral $[PO_4]^{3-}$ anions. Hence, the observed frequencies are closely related to those of the free phosphate molecule [46]. In the spectrum, four fundamental vibrations are present: symmetric bending vibrations (doublet) of O–P–O (ν_2 at 466–644 cm^{-1}), antisymmetric bending vibrations of the O–P–O fragment (ν_4 around 644 cm^{-1}), asymmetric stretching vibrations (triplet) of P–O (ν_3 around 1058 cm^{-1}), and symmetric stretching vibrations of P–O bond (ν_1 967–1146 cm^{-1}). Out of these, only the vibrations ν_2 and ν_3 are infrared active. However, theoretically non-active vibrations can be observed. Hence, a band due to symmetric stretching vibration around 937–970 cm^{-1} and a band due to deformation vibrations around 358–420 cm^{-1} are expected in some cases [47,48]. Table S4 resumes the assignments of the IR vibrations. Here, two main regions can be distinguished: The first between 400 and 700 cm^{-1} is associated with the intramolecular $[PO_4]^{3-}$ bending modes (ν_2 and ν_4); the region from 900 to 1200 cm^{-1} corresponds to the intramolecular stretching vibrations of the tetrahedral anion (ν_1 and ν_3). Furthermore, the spectrum shows a splitting in the relative intensities of the intramolecular $[PO_4]^{3-}$ bands due to the difference of the specific interactions between the diverse ions and the unit cell, specifically between the monovalent lithium ion and the phosphate anion [48]. In addition to that, the bands below 500 cm^{-1} could be attributed to Li-ion "cage modes," which represent translational vibrations of the Li-ions inside a potential energy environment determined by the neighbor oxygen atoms; however, due to splitting effect, this bands are overlapping with the phosphate bending vibrations [49].

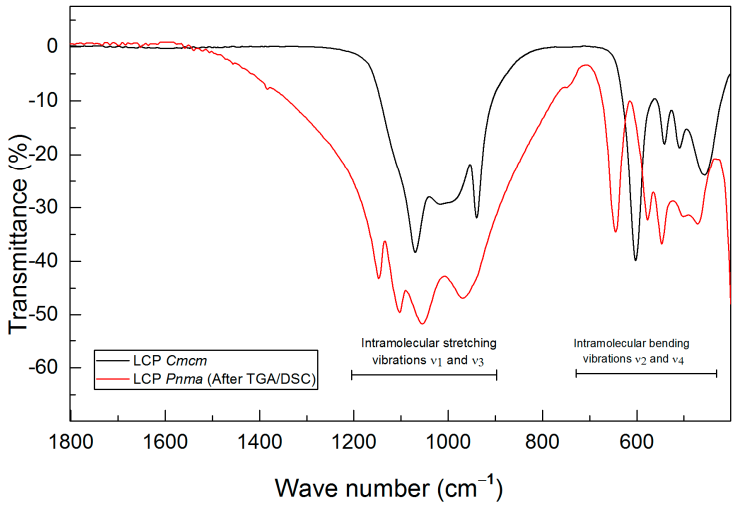

Figure S2. Comparison of the FTIR spectra of (**a**) the *Cmcm*-LCP (PO) obtained from the polyol route (**black**); and (**b**) *Pnma*-LCP obtained after the TGA/DSC measurement at 900 °C (**red**).

Table S4. Assignments of the internal and external IR vibrations for (a) LCP-*Cmcm* (PO) and (b) LCP-*Pnma* obtained after the TGA/DSC experiment.

	FT-IR Assignment	**Frequency (cm^{-1})**	
	Vibrational mode	**(a) LCP-*Cmcm***	**(b) LCP-*Pnma***
Intramolecular bending modes	Li^+ ion "cage modes"	457	470
	Symmetric bending vibration O–P–O	511	501
		541	547
	Asymmetric stretching modes [CoO_6] octahedra	603	577
	Asymmetric bending vibration O–P–O	-	646
Intramolecular stretching modes	Symmetric stretching vibrations P–O	941	970
	Asymmetric stretching vibrations P–O	1002	1050
	Asymmetric stretching vibration P=O	1071	1103
		–	1147

1.3. Temperature-Dependent In Situ X-Ray Powder Diffraction

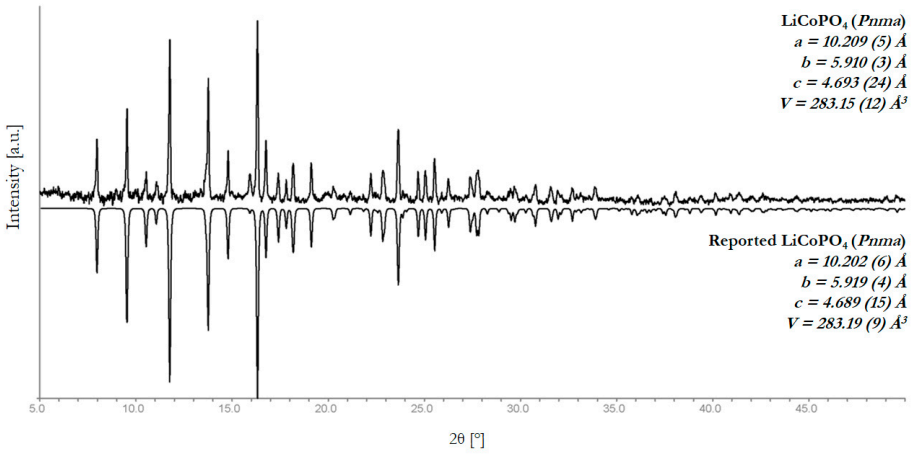

Figure S3. Room temperature PXRD of a LCP-*Cmcm* (PO) sample after the temperature-dependent in situ PXRD experiment. Heating to 800 °C and cooling to room temperature resulted in LCP-*Pnma* as the final product.

Table S5. Temperature program used for temperature-dependent PXRD measurements.

Temperature Range			Heating Rate
20 °C	to	200 °C	(50 °C/min)
200 °C	to	300 °C	(50 °C/min)
300 °C	to	350 °C	(10 °C/min)
350 °C	to	400 °C	(10 °C/min)
400 °C	to	425 °C	(2° C/min)
425 °C	to	450 °C	(2° C/min)
450 °C	to	475 °C	(2° C/min)
475 °C	to	500 °C	(2° C/min)
500 °C	to	525 °C	(10 °C/min)
525 °C	to	550 °C	(10 °C/min)
550 °C	to	575 °C	(10 °C/min)
575 °C	to	600 °C	(10 °C/min)
600 °C	to	625 °C	(10 °C/min)
625 °C	to	650 °C	(10 °C/min)
650 °C	to	675 °C	(10 °C/min)
675 °C	to	700 °C	(10 °C/min)
700 °C	to	725 °C	(10 °C/min)
725°C	to	750 °C	(10 °C/min)
750 °C	to	775 °C	(10 °C/min)
775 °C	to	800 °C	(10 °C/min)